Simultaneous High-Speed Tomography and Schlieren Measurements of Spherically Expanding Methane/Air Flames

Joachim Beeckmann[a], Emilien Varea[a,b], André Berens[a], Bruno Renou[b], Heinz Pitsch[a]

[a] *Institute for Combustion Technology, RWTH Aachen University, 52056 Aachen, Germany*
[b] *CORIA-UMR 6614, Normandie Université, CNRS, INSA et Université de Rouen Av de l'Université, 76800 Saint Etienne du Rouvray, France*

Abstract

Laminar burning velocities are of great importance for turbulent combustion (flame speed scaling) as well as validation and improvement of chemical kinetic schemes. Determining laminar burning velocities with high accuracy is quite challenging and different approaches exist. Hence, a comparison of existing methods measuring the laminar burning velocity based on different optical diagnostics is interesting, but not straightforward, since the intrinsic uncertainties associated to each setup are not well known. In this study, two optical diagnostics are simultaneously set up to investigate laminar flame speed in a spherical flame configuration. The two techniques are high speed tomography and Schlieren cinematography. The latter is representative for most optical flame speed measurement setups. Therefore, direct comparison of the two techniques allows highlighting the differences in flame speed and in measured Markstein lengths, which represents the flame sensitivity to stretch. The measurements of spherically expanding flames are carried out in a high-pressure, high-temperature constant-volume vessel. A methane / air mixture is chosen for the experiments with an equivalence ratio of 1.1 at a temperature and pressure of 298 K and 2.5 bar, respectively. The unstretched laminar flame speed with respect to the burnt is found to be strictly the same with the two methods, although the flame speed over stretch, and correspondingly the Markstein length, differs significantly. The importance of the isothermal reference for flame speed calculation is discussed.

Keywords: Methane; High-Speed Tomography; Schlieren; Laminar Burning Velocity; Spherical Flames

1. Introduction

Laminar burning velocities are of great importance for turbulent combustion as well as validation and improvement of chemical kinetic schemes [1]. Determining laminar burning velocities with high accuracy is quite challenging. Different experimental configurations exist, such as spherically expanding flames [2–5], counterflow flames [6–9], the heat flux method [10, 11], or Bunsen flames [12–14]. The spherically expanding flame configuration (SEF) is generally used, since it offers flexibility in terms of initial pressure, temperature and gas composition. Even though SEF studies started now almost one hundred years ago, comparison between different experimental data sets is still quite challenging. Flame recording techniques (pressure trace, Schlieren cinematography, high speed shadowgraphy or tomography techniques) as well as chamber geometries may differ from one setup to another. Hence, a comparison of existing methods for determining the laminar flame speed based on different optical diagnostics is interesting, but not straightforward, since the intrinsic uncertainties associated to each setup are not well known. In this study, outwardly propagating spherical flames are examined experimentally with simultaneous high-speed tomography and Schlieren imaging. In both techniques, the flame radius evolution over time $\Delta r/\Delta t$ is recorded. High-speed tomography

* Corresponding author: Joachim Beeckmann
j.beeckmann@itv.rwth-aachen.de
Proceedings of the European Combustion Meeting 2015

allows determining the flame position based on the evaporation contour of oil droplets. Additionally, the fresh gas velocity at the entrance of the flame front can be measured through particle image velocimetry (piv). This data can be used in a kinematic relationship to obtain the flame speed with respect to the unburnt [3]. The Schlieren imaging technique on the other hand uses the flame location close to the reaction rate peak (highest refraction optical index). The objectives of this work are i/ to simultaneously compare the flame displacement speed with respect to the burnt obtained by two different optical diagnostics, and ii/ to evaluate the Markstein lengths and unstretched burning velocities from the two methods. In the next section (Section 2) the experimental setups and the optical diagnostics are presented. The determination of the flame speed is discussed in Section 3, and Section 4 shows the results and provides a discussion. The work is summarized and concluded in section 5.

2. Experimental Setup and Conditions

Experiments were performed using the closed-vessel method combined with an optical Schlieren cinematography setup, comparable to the one described by Beeckmann et al. [4]. Simultaneously, a tomography setup, comparable to the one described by Varea et al. [3], is used. Both optical diagnostic setups allow measuring the flame front evolution (radius) at elevated pressure and temperature. The experimental setup is shown schematically in Figure 1. The internal shape of the combustion vessel is spherical with an inner diameter of 100 mm; quartz windows with a diameter of 50 mm are positioned on opposite sides [4]. To allow the simultaneous application of the tomography and Schlieren system, an additional cylindrical spacer of 30 mm width is placed between the two half shells of the sphere. The spacer is equipped with two rectangular quartz windows positioned on opposite sides. The optical access is 45 mm in height and 10 mm in width.

The Schlieren setup images the outward location of the propagating flame using a dual-field-lens Schlieren arrangement [15]. It is combined with a high-speed CMOS camera (LaVision HighSpeedStar 6). Images were taken with 5000 frames per second (fps), at a full frame resolution of 1024x1024 pixels, an exposure time of 1/104000 s,

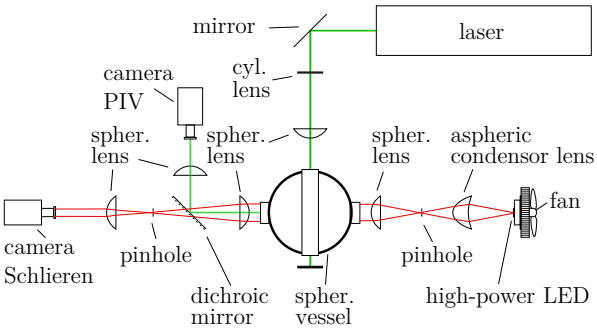

Figure 1: Schematic of the experimental setup

and a pixelsize of 0.0383 mm/pixel. The Schlieren system consists of a continuous high power LED as a light source and an adjustable power output. The LED, type Luminus CBT-120-R-C11-HM101, BM-R5 [16], emits red light with a dominant wavelength of 622 nm. Power output is set to a voltage and current of 2.3 V and 4.2 A, respectively. Optical lenses are an aspheric condenser lens and three spherical lenses. Two pinholes with a diameter of 0.5 mm are used. Overexposure of the camera from flame radiation is prevented by an optical filter.

The tomographic setup uses a double head, high-speed Nd:YLF laser (Litron LDY303HE) to illuminate seeding particles. The laser emits green light at a wavelength of 527 nm with a power output of 35.1 W at 5 kHz. The two cavities are run simultaneously to prevent shot to shot intensity variations of each individual cavity. The laser sheet is created by associating one cylindrical lens and one spherical lens. A high-speed CMOS camera of the same type as used for the Schlieren setup (LaVision HighSpeedStar 6) records images at 5000 frames per second (fps), at a full frame of 1024x1024 pixels, an exposure time of 1/62000 s, and a pixel-size of 0.0426 mm/pixel. The tomography camera captures the Mie scattering signal from particles via an dichroic mirror, with a reflection band of the green light bigger than 90 %. An interferential pass band filter (527±10 nm) mounted to the camera lens removes any flame chemiluminescence as well as residual red light from the LED. To capture the tomography images, the combustion vessel is seeded with olive oil droplets, which vaporise at a temperature of about 580 K. This boiling point temperature is high enough for the seeding droplets to exist well into the preheat zone and can be used to capture the maximum velocity point upstream of the flame. This is important for future work dealing

with the measurement of the fresh gas velocity just ahead of the flame [3]. A separate mixing vessel is employed for an external preparation of the gas mixture. It is connected directly to the combustion chamber via pipes. While filling the combustion vessel with air / fuel mixture, parts of the mixture stream is led through a particle seeder for seeding the mixture with oil droplets. The fuel storage, the external mixing vessel, all pipes in contact with fuel, the PIV seeder, and the combustion vessel can be also heated to prevent fuel condensation, if liquid instead of gaseous fuels are used for experiments. The amount of fuel needed can be calculated as a function of ϕ, T, and p. The partial pressure method can be used for accurately measuring and controlling the filling process. In addition, a real gas correction has been applied by using the Soave modification of the Redlich–Kwong equation of state [17].

Before sparking, the mixture is allowed to settle. A two-step ignition system is used for igniting the mixture at the midpoint of the vessel with extended spark plug electrodes of 1 mm diameter.

The present experimental setup was verified against methane / air and ethanol / air laminar burning velocities at various pressures, temperatures, and equivalence ratios [4, 18].

In this study, methane / air flames with an equivalence ratio of 1.1 at a pressure of 2.5 bar and a temperature of 298 K are investigated. Experimental conditions were set up with compressed air, which consists in 20.94 % oxygen, 78.13 % nitrogen, and 0.93 % argon. Methane is sourced from Westfalen gas, grade 5.5.

3. Determination of Flame Speeds

The image post-processing of the propagating flame, performed under the assumption of constant pressure, yields information of the expanding flame radius r_f over time t. As flame images for Schlieren and tomography technique look different, two separate radius extraction routines are employed. The flame radius is extracted from the captured Schlieren images using a grey level threshold method by Otsu et al. [19] and for the tomography images an adaptive threshold method is applied [20]. The stretched propagation speed with respect to the burnt mixture S_b can then be determined by

$$S_b = \frac{\mathrm{d}r_f}{\mathrm{d}t}, \tag{1}$$

applying a central difference scheme. The evaluation of the observed experimental data was restricted to spherical smooth flame fronts with a radius above 7 mm in order to avoid the spark's influence as a result of the ignition process [21–24]. The stretch rate κ is defined as the temporal change of a flame surface area A [25]. In case of a spherically outwardly expanding flame front, κ can be expressed as

$$\kappa = \frac{1}{A}\frac{\mathrm{d}A}{\mathrm{d}t} = \frac{2}{r_f}\frac{\mathrm{d}r_f}{\mathrm{d}t}. \tag{2}$$

The response of flames to stretch has been analysed on the basis of an asymptotic analysis by Clavin and Williams [26], Pelce and Clavin [27], and Matalon and Matkowsky [28].

In this study, a non-linear model has been utilized to extract the unstretched laminar flame speed, S_b^0, and the Markstein length, L_b . This technique has been discussed by Halter et al. [2], is based on an earlier work of Ronney and Sivashinsky [29], and is given

$$\left(\frac{S_b}{S_b^0}\right)^2 \ln\left(\frac{S_b}{S_b^0}\right)^2 = -\frac{2L_b\kappa}{S_b^0}. \tag{3}$$

The burnt flame speed S_b is plotted against the stretch rate κ. A least-squares fit is applied to obtain the unknows, S_b^0 and L_b. As a result, the following expression is minimised:

$$\sum_{i=m}^{N} \left| \left(\frac{S_b}{S_b^0}\right)^2 \ln\left(\frac{S_b}{S_b^0}\right)^2 + \frac{2L_b\kappa}{S_b^0} \right|, \tag{4}$$

where N corresponds to the number of discrete observation times.

The laminar burning velocity S_L is defined as the unstretched flame displacement speed with respect to the unburnt mixture, S_u^0. It can be determined from mass continuity through a planar unstretched flame as

$$S_L = S_u^0 = S_b^0(\rho_b/\rho_u). \tag{5}$$

Here, ρ_b and ρ_u are the densities of the burnt and unburnt mixture. ρ_b is evaluated at adiabatic flame temperature conditions.

4. Results and Discussion

The experimental results for the unstretched flame speed with respect to the burnt for the tomography and the Schlieren method are presented and discussed in this section. Images of the spherical

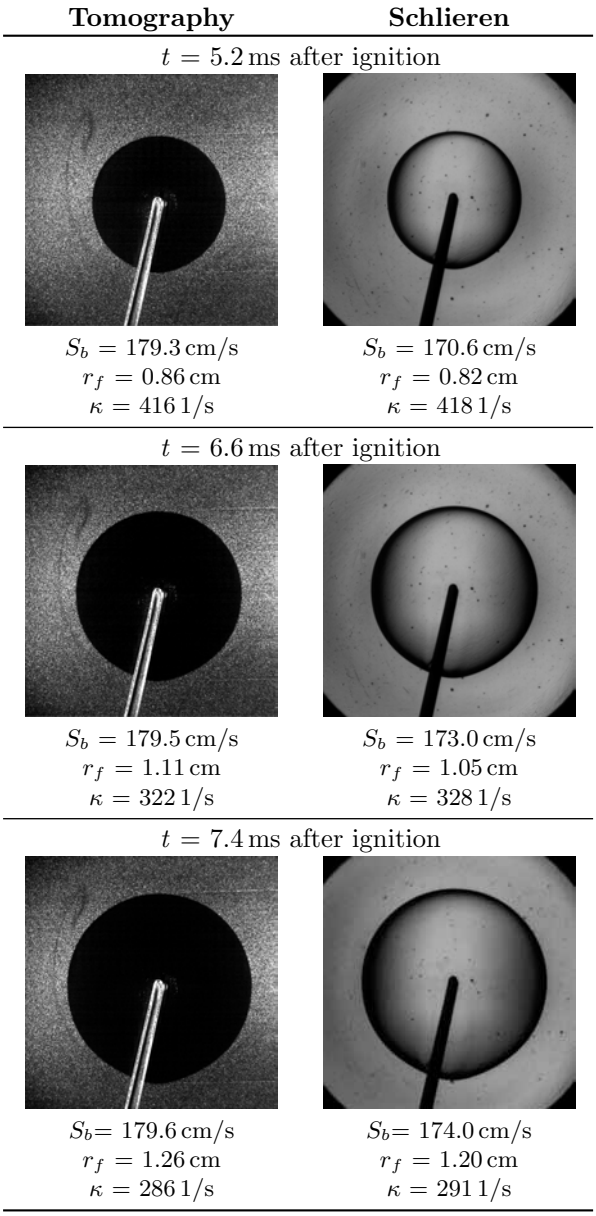

Figure 2: Captured images of spherical methane / air flames at $\phi = 1.1$, $p = 2.5$ bar, and $T_i = 298$ K; tomography (left column) and Schlieren (right column).

flames of the methane / air mixture are shown in Figure 2. Images are taken at three different times after ignition: 5.2 ms, 6.6 ms, and 7.4 ms. The left column shows the tomographic images and the right column shows for exactly the same times the corresponding Schlieren images. In addition, the flame propagation speed S_b and the stretch rate κ are given. The elongated electrodes of the spark plug are positioned in the centre of the combustion vessel. As one can see from the Schlieren images, the flame surface remains smooth throughout the entire visible flame radius evolution without any observable flame disturbances or instabilities. In addition, the constraint of quasi isobaric conditions for post-processing is taken into account to correctly estimate the laminar burning velocity with respect to the unstretched flame displacement speed in the unburnt. For the present experimental condition, the flame radii of the Schlieren images are always marginally smaller than the tomographic ones. The differences are on the order of the flame thickness. The flame consumption speed for the tomography has a marginal rise, indicating a small Markstein length, while for the Schlieren technique, the rise in flame speed is slightly higher over time. This behaviour is also illustrated in Figure 3, where the corresponding flame speed extractions over stretch are shown for the two acquisition methods. The temporal evolution goes from high to low stretch values. Symbols indicate the results of the post-processed flame images. Solid lines represent the non-linear extrapolation according to Eq. 3.

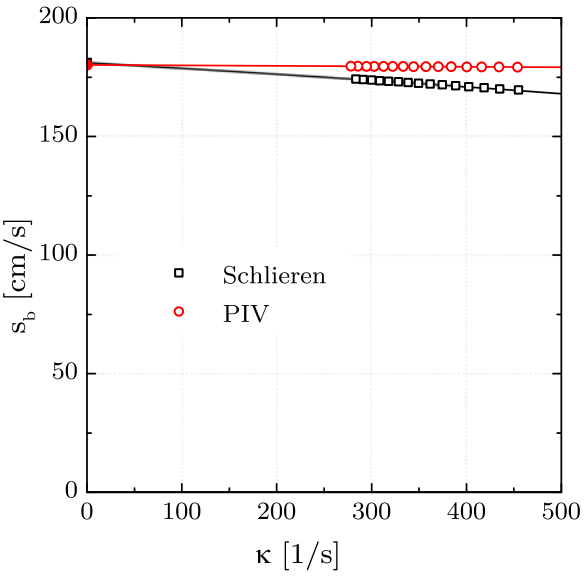

Figure 3: Measured flame propagation speed over stretch rate; Schlieren (hollow squares) and tomography (hollow circles); non-linear extrapolation for Schlieren (black line) and tomography (red line); $\phi = 1.1$, $p_i = 2.5$ bar, and $T_i = 298$ K.

The results for the unstretched flame displacement speed with respect to the burnt are for the Schlieren method 181.1 cm/s and for the tomogra-

phy 180.2 cm/s. These are, from an experimental point of view, identical results, with a negligible difference of less than 0.5%. The slopes of the extrapolations differ from each other, leading to Markstein lengths for the Schlieren and the tomography of 0.2298 mm and 0.0199 mm, respectively. The origin of two separate Markstein lengths lies in the temperature isosurface representing the flame front for the flame radius estimation. Giannakopoulos et al. [30] have investigated the dependence of Markstein length on temperature isosurfaces by computations. Variations of the temperature isosurface within the reaction zone ($T \gtrsim 4.5 \cdot T_u$, where subscript u refers to the unburnt) converge to almost the same slope corresponding to the same burnt Markstein length. On the other hand, variations of the temperature isosurface within the preheat zone ($1.01 \cdot T_u \leq T \lesssim 4 \cdot T_u$) exhibit a larger spread in Markstein lengths [30]. For the first time, experiments quantitatively show simultaneously the differences in Markstein length depending on the measurement technique.
Finally, the laminar burning velocity is deduced by using the mass continuity over the flame front. In addition, the flame speed for the measured experimental condition in this study is also computed. The calculations for density ratio and flame speed are performed with the FlameMaster [31] software package. The kinetic mechanism, transport data, and thermodynamic properties are taken from the GRI 3.0 [32]. Here, the density ratio is 0.01323. Laminar burning velocities of the Schlieren technique, the tomography, and simulations do agree extremely well. They result in 23.96 cm/s, 23.84 cm/s, and 23.81 cm/s, respectively.
In conclusion, the two techniques measure the same unstretched flame displacement speed with respect to the brunt and unburnt. The Schlieren technique measures the Markstein length in the burnt using a temperature isosurface in the reaction zone, whereas a Markstein length corresponding to an iso-surface in the in the unburnt is quantified by the tomography technique. It is associated to a moving isothermal surface close to a temperature in the preheat zone, which depends strongly on the evaporation behaviour of the oil droplets.

5. Concluding Remarks

In this work, an experimental setup is presented to measure for the first time flame displacement speed with a high-speed Schlieren and a high-speed tomography method simultaneously in a spherical combustion vessel. A methane / air mixture of $\phi = 1.1$ at a temperature of 298 K and a pressure of 2.5 bar is chosen for experiments. The unstretched flame displacement speed with respect to the burnt is found to be the same for the two techniques. Two different Markstein lengths are found for the two acquisition methods. The tomographic Markstein length is smaller than that from Schlieren imaging. This is due to different temperature isosurfaces used for image acquisition. More simultaneous measurements for validation are needed to investigate equivalence ratio, initial pressure and temperature, and fuel effects on the Markstein length. One goal will be the comparison to results from a joint collaborative verification study presented in [18] for ambient temperature and pressure with equivalence ratios of 0.8, 1.1, and 1.3. In addition, the laminar burning velocities obtained directly by the kinematic relationship of the flame displacement speed and the fresh gas velocity near the preheat zone of the flame front via tomography should be closely compared to the laminar burning velocities deduced with the density ratio by the Schlieren method.

Acknowledgements

This work was performed as part of the Cluster of Excellence "Tailor-Made Fuels from Biomass", which is funded by the Excellence Initiative of the German federal and state governments to promote science and research at German universities.
B. Renou and E. Varea thank the European Regional Development Fund under Grant Interreg IV E3C3.

References

[1] Norbert Peters. *Turbulent Combustion*. Cambridge University Press, 2000. Cambridge Books Online.
[2] F. Halter, T. Tahtouh, and C. Mounaïm-Rousselle. Nonlinear effects of stretch on the flame front propagation. *Combustion and Flame*, 157(10):1825–1832, 2010.
[3] E. Varea, V. Modica, A. Vandel, and B. Renou. Measurement of laminar burning velocity and Markstein length relative to fresh gases using a new postprocessing procedure: Application to laminar spherical flames for methane, ethanol and isooctane/air mixtures. *Combustion and Flame*, 159(2):577–590, 2012.
[4] J. Beeckmann, L. Cai, and H. Pitsch. Experimental investigation of the laminar burning velocities of methanol, ethanol, n-propanol, and n-butanol at high pressure. *Fuel*, 117, Part A(0):340–350, 2014.

[5] F. Halter, C. Chauveau, N. Djebaili-Chaumeix, and I. Gokalp. Characterization of the effects of pressure and hydrogen concentration on laminar burning velocities of methane-hydrogen-air mixtures. *Proceedings of the Combustion Institute*, 30:201–208, 2005.

[6] Y. Dong, C.M. Vagelopoulos, G.R. Spedding, and F.N. Egolfopoulos. Measurement of laminar flame speeds through digital particle image velocimetry: Mixtures of methane and ethane with hydrogen, oxygen, nitrogen, and helium. *Proceedings of the Combustion Institute*, 29(2):1419 – 1426, 2002.

[7] Y. Huang, C.J. Sung, and J.A. Eng. Laminar flame speeds of primary reference fuels and reformer gas mixtures. *Combustion and Flame*, 139:239–251, 2004.

[8] C.M. Vagelopoulos and F.N. Egolfopoulos. Direct experimental determination of laminar flame speeds. *Proceedings of the Combustion Institute*, 27:513–519, 1998.

[9] C.M. Vagelopoulos, F.N. Egolfopoulos, and C.K. Law. Further considerations on the determination of laminar flame speeds with the counterflow twin-flame technique. *Proceedings of the Combustion Institute*, 25:1341–1347, 1994.

[10] R.T.E. Hermanns. PhD thesis, TU Eindhoven, 2007.

[11] K.J. Bosschaart and L.P.H. de Goey. Detailed analysis of the heat flux method for measuring burning velocities. *Combustion and Flame*, 132(1-2):170 – 180, 2003.

[12] B. Lewis and G. von Elbe. *Combustion, Flames and Explosions of Gases*. Academic Press, 3rd edn. edition, 1987.

[13] O. Kurata, S. Takahashi, and Y. Uchiyama. Influence of Preheat Temperature on the Laminar Burning Velocity of Methane-Air Mixtures. *SAE Technical Paper*, 1994.

[14] Y. Ogami and H. Kobayashi. Laminar burning velocity of stoichiometric CH4/air premixed flames at high-pressure and high-temperature. *JSME International Journal Series B*, 48:603–609, 2006.

[15] Gary S. Settles. *Schlieren and Shadowgraph Techniques: Visualizing Phenomena in Transparent Media*, volume 2. Springer Berlin, 2001.

[16] Luminus Devices, Inc. *CBT-120 Product Datasheet*, 2011.

[17] B. Poling, J. Prausnitz, and J.O. Connell. *The Properties of Gases and Liquids*. McGraw Hill professional. Mcgraw-hill, 2000.

[18] J. Beeckmann, N. Chaumeix, P. Dagaut, G. Dayma, F. Foucher, F. Halter, A. Lefebvre, C. Mounaim-Rousselle, H. Pitsch, B. Renou, and E. Varea. Collobartive study for accurate measurements of laminar burning velocity. *6th European Combustion Meeting, Lund, Sweden*, 2013.

[19] N. Otsu. A threshold selection method from gray-level histograms. *IEEE transaction on systems and cybernetics*, 9(1):62–66, 1979.

[20] G. Bradski. The opencv library. *Dr. Dobb's Journal of Software Tools*, 2000.

[21] Z. Chen, M.P. Burke, and Y. Ju. Effects of Lewis number and ignition energy on the determination of laminar flame speed using propagating spherical flames. *Proceedings of the Combustion Institute*, 32(1):1253–1260, 2009.

[22] D. Bradley, P.H. Gaskell, and X.J. Gu. Burning velocities, Markstein lengths, and flame quenching for spherical methane-air flames: a computational study. *Combustion and Flame*, 104(1):176–198, 1996.

[23] D. Bradley, R.A. Hicks, M. Lawes, C.G.W. Sheppard, and R. Woolley. The measurement of laminar burning velocities and Markstein numbers for iso-octane–air and iso-octane–n-heptane–air mixtures at elevated temperatures and pressures in an explosion bomb. *Combustion and Flame*, 115(1):126–144, 1998.

[24] A.Y. Starikovskii. Plasma supported Combustion. *Proceedings of the Combustion Institute*, 30(2):2405–2417, 2005.

[25] F.A. Williams. *Combustion theory : the fundamental theory of chemically reacting flow systems*. Combustion science and engineering series. Menlo Park, Calif. Benjamin/Cummings Pub. Co. c1985, 1985.

[26] P. Clavin and F.A. Williams. Effects of molecular diffusion and of thermal expansion on the structure and dynamics of premixed flames in turbulent flows of large scale and low intensity. *Journal of Fluid Mechanics*, 116:251–282, 1982.

[27] P. Pelce and P. Clavin. Influence of hydrodynamics and diffusion upon the stability limits of laminar premixed flames. *Journal of Fluid Mechanics*, 124:219–237, 1982.

[28] M. Matalon and B.J. Matkowsky. Flames as gasdynamic discontinuities. *Journal of Fluid Mechanics*, 124:239–259, 1982.

[29] P.D. Ronney and G.I. Sivashinsky. A theoretical study of propagation and extinction of nonsteady spherical flame fronts. *SIAM Journal on Applied Mathematics*, 49(4):1029–1046, 1989.

[30] G.K. Giannakopoulos, A. Gatzoulis, C.E. Frouzakis, M. Matalon, and A.G. Tomboulides. Consistent definitions of "'flame displacement speed"' and "'markstein length"' for premixed flame propagation. *Combustion and Flame*, (0), 2014.

[31] H. Pitsch. Flamemaster: A C++ computer program for 0D combustion and 1D laminar flame calculations. 1998.

[32] G. Smith, D. Golden, M. Frenklach, N. Moriarty, B. Eiteneer, M. Goldenberg, T. Bowman, R. Hanson, S. Song, W. Gardiner, V. Lissianski, and Q. Zhiwei, 2009. University of California, CA.